STRAIN CALCULATIONS FOR CIRCUMFERENTIAL GRABEN ON ALBA MONS, MARS

Teemu Öhman and Patrick J. McGovern

Lunar and Planetary Institute, Universities Space Research Association, 3600 Bay Area Blvd., Houston, TX 77058, USA. ohman@lpi.usra.edu, mcgovern@lpi.usra.edu

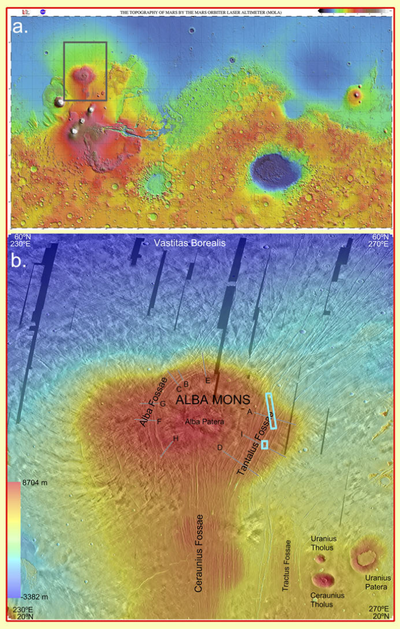

Fig. 1. The location of a.) Alba Mons and b). the transects across the flank graben. Cyan boxes indicate the locations of Fig. 5 (upper; Fig. 3 is inside it) and Fig. 4 (lower). Width of view at the center ~1800 km. MOLA 128 px/deg DEM on THEMIS IR daytime 100 m/px mosaic.

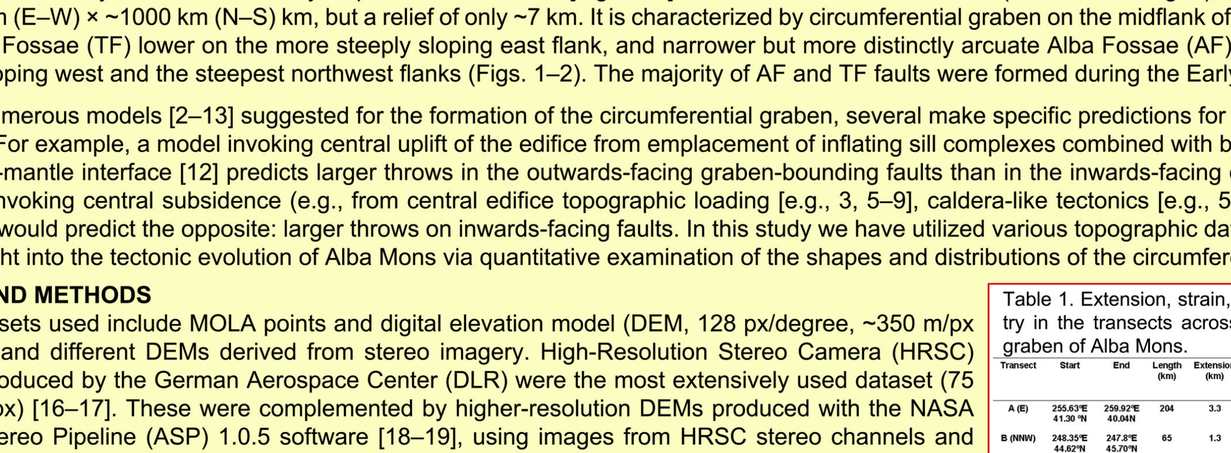

Fig. 2. The throws (vertical components of displacement) of graben and normal faults. The diagrams on the map show the difference of throw between outwards- and inwards-facing faults (outwards minus inwards; white = outwards > inwards, blue = outwards < inwards), whereas the separate larger diagrams display the actual throw itself (white = outwards-facing, blue=inwards-facing). Note that in the separate diagrams F–H the summit of the volcano is to the right, whereas in all others it is to the left. For scale, transects C and F are ~100 km long (see Table 1).

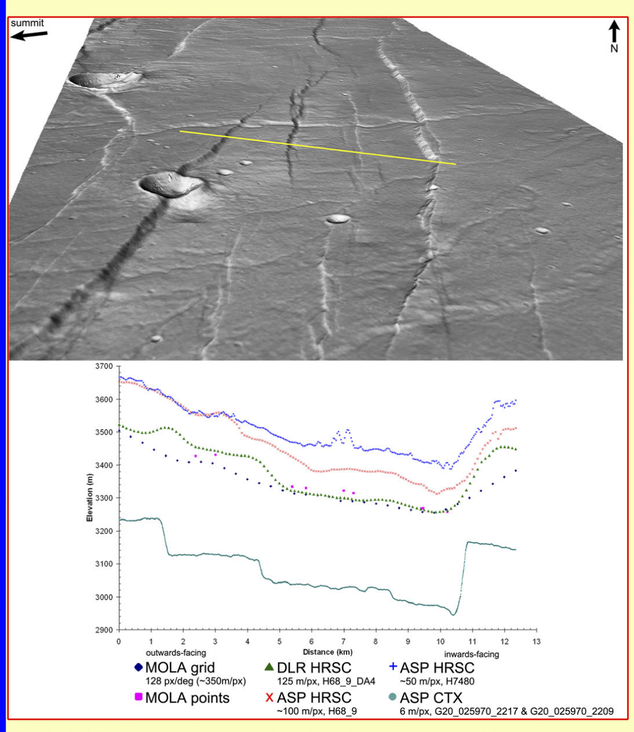

Fig. 3. A CTX perspective view of profile A5, created with ASP, on the eastern flank of Alba Mons (see Fig. 1 for location). MOLA DEM entirely misses the nested graben, DLR DEM smoothens the topography too much, and ASP HRSC DEMs tend to be noisy and misplace the nested graben. ASP CTX DEM provides the most realistic depiction of the profile topography. Bundle adjustment or control points were not used in the making of the DEMs with ASP, which creates differences in the absolute elevations, but the relative elevations (throws) in different DEMs are broadly consistent.
CTX images G20_025970_2217_XN_41N102W.IMG and G20_025904_2209_XN_40N102W.IMG.

INTRODUCTION AND GEOLOGIC BACKGROUND

Alba Mons is a very broad but shallowly sloped volcanic edifice [e.g., 1–3] north of the Tharsis rise, Mars (40ºN 250ºE; Fig. 1), with a diameter of ~1400 km (E–W) × ~1000 km (N–S) km, but a relief of only ~7 km. It is characterized by circumferential graben on the midflank of the edifice; wider Tantalus Fossae (TF) lower on the more steeply sloping east flank, and narrower but more distinctly arcuate Alba Fossae (AF) higher up on the gently sloping west and the steepest northwest flanks (Figs. 1–2). The majority of AF and TF faults were formed during the Early Amazonian [4].

Of the numerous models [2–13] suggested for the formation of the circumferential graben, several make specific predictions for the distribution of faulting. For example, a model invoking central uplift of the edifice from emplacement of inflating sill complexes combined with buoyant loading at the crust-mantle interface [12] predicts larger throws in the outwards-facing graben-bounding faults than in the inwards-facing ones. In contrast, models invoking central subsidence (e.g., from central edifice topographic loading [e.g., 3, 5–9], caldera-like tectonics [e.g., 5], or dense cores [e.g., 5]) would predict the opposite: larger throws on inwards-facing faults. In this study we have utilized various topographic datasets to gain further insight into the tectonic evolution of Alba Mons via quantitative examination of the shapes and distributions of the circumferential graben.

DATA AND METHODS

The datasets used include MOLA points and digital elevation model (DEM, 128 px/degree, ~350 m/px [14–15]) and different DEMs derived from stereo imagery. High-Resolution Stereo Camera (HRSC) DEMs produced by the German Aerospace Center (DLR) were the most extensively used dataset (75–150 m/px) [16–17]. These were complemented by higher-resolution DEMs produced with the NASA Ames Stereo Pipeline (ASP) 1.0.5 software [18–19], using images from HRSC stereo channels and Mars Reconnaissance Orbiter Context Camera (CTX; see Fig. 3 for a comparison). As the graben are typically asymmetric ([20–21], Figs. 3–5) throws were measured separately for the inwards- and outwards-facing graben-bounding faults. For the calculation of horizontal extension, we assumed a 60º fault angle: extension = apparent throw / tan 60º. Total extensional strains along the length of the transects were calculated as: strain = Σheave / (transect length – Σheave). As the calculations are based on apparent throws, which is less than the original throw due to erosion, sedimentation, and profiles not always being exactly perpendicular to strike, the calculated extension and strain should be considered as minima.

Table 1. Extension, strain, and throw asymmetry in the transects across the circumferential graben of Alba Mons.

Transect	Start	End	Length (km)	Extension (km)	Strain (%)	Inwards / outwards throw (%)	Outwards – inwards throw / relief (%)*
A (E)	255.63°E 41.30 °N	259.92°E 40.04N	204	3.3	1.6	84	16
B (NNW)	248.35°E 44.62°N	247.8°E 45.70°N	65	1.3	2.0	72	16
C (NNW)	247.84°E 44.13°N	246.76°E 45.63°N	97	1.9	2.0	73	19
D (SE)	252.40°E 37.38°N	256.12°E 34.80°N	233	3.8	1.7	76	40
E (N)	250.65°E 45.00°N	250.28°E 47.49°N	147	1.2	0.8	46	19
F (W)	245.57°E 40.50°N	243.39°E 40.59°N	98	0.8	0.8	104	-19
G (W)	245.86°E 42.25°N	243.91°E 42.24°N	84	1.2	1.4	101	36
H (SW)	247.28°E 38.34°N	246.04°E 36.75°N	108	0.5	0.5	76	10
I (ESE)	254.59°E 38.95°N	258.93°E 36.71°N	242	2.6	1.1	85	15

*Indicates how large percentage the total cumulative throw difference (outwards-inwards) makes of the total elevation difference between the starting and ending points of the transect.

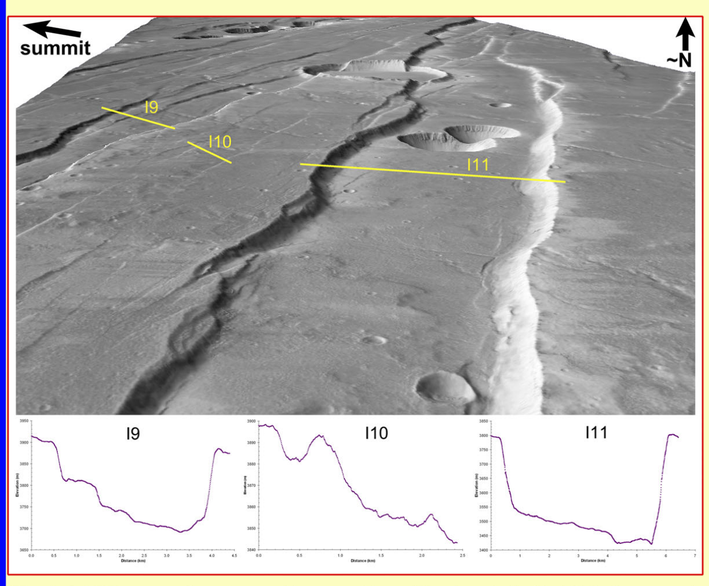

Fig. 4. A CTX perspective view and topographic profiles (created with ASP) of asymmetric graben on the eastern flank of Alba Mons (see Fig. 1 for location). Note the varying scales of the profiles. CTX images B21_017900_2183_XI_38N103W.IMG and B20_017399_2183_XI_38N103W.IMG

RESULTS AND PRELIMINARY CONCLUSIONS

The throws (and, thus, horizontal extensions) measured from the transects form distinct groups, based on their location. In most of the transects (A–D, H–I), the total cumulative throws from inwards-facing faults are from 72% to 85% of the outwards-facing throws. On the northern, steeply sloping transect (E) the total inwards-facing throw is only 46% of the outwards-facing throw (Table 1). Only on the western, very shallowly sloping transects (F and G; Fig. 2) are the total cumulative throws from the inwards-facing faults slightly larger than from the outwards-facing ones (101–104%, or 13–26 m). Similarly, the total extensional strains are notably different in different parts of Alba Mons. The largest strains of ~2% are encountered in the north-northwest transects (B and C), while the southwestern flank of Alba Mons (transect H) shows strain of only ~0.5% (Table 1). The highest throws of individual profiles, over 600–700 m, are found in the outwards-facing faults of the uppermost graben in the north-northwest transects (B and C; Fig. 2). On the eastern flank (transect A), our measurements indicate a strain about twice as large as determined by Polit et al. [21], most likely due to the higher resolution of our data.

These observations generally favor models with expansion and uplift [e.g., 12, 22–23] rather than contraction and subsidence. The measured strain of ~0.5–2% is consistent with sill complex emplacement with overall thickness of several km late in the history of the edifice [12]. However, the minor concentration of larger throw from inwards-facing faults on the upper part of the flanks may imply an additional late phase of minor subsidence due to summit loading, consistent with a multi-stage evolution model [e.g., 3].

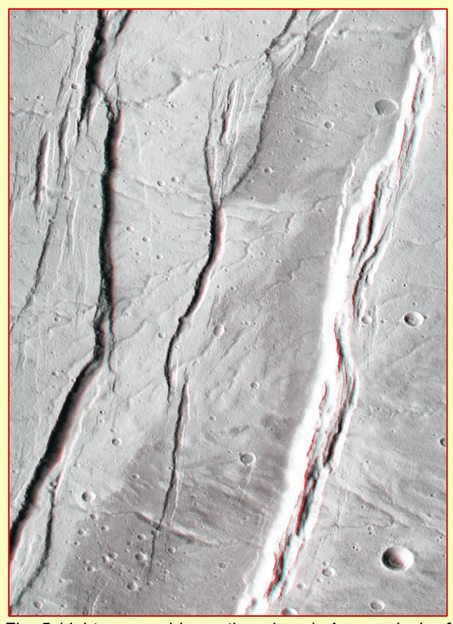

Fig. 5 (right, zoomed in section above). An anaglyph of graben on eastern Alba Mons (see Fig. 1). Elliptical shape of the craters is mostly due to simple cylindrical projection. CTX images G20_025970_2217_XN_41N102W.IMG and G20_025904_2209_XN_40N102W.IMG.

Acknowledgements: This project was supported by NASA Mars Data Analysis Program (MDAP) grant NNX09AI42G.

References: [1] Carr M. (1973) *JGR, 78,* 4049–4062. [2] Wise D. (1979) Geologic Map of the Arcadia Quadrangle of Mars, Map I-1154, USGS. [3] Ivanov M. and Head J. (2006) *JGR, 111,* E09003. [4] Tanaka K. (1990) *PLPSC, 20,* 515–523. [5] Cailleau B. et al. (2003) *JGR, 108,* 5141. [6] Comer R. et al. (1985) *Rev. Geophys., 23,* 61–92. [7] Raitala J. (1988) *EMP, 42,* 277–291. [8] Turtle E. and Melosh H. (1997) *Icarus, 126,* 197–211. [9] Raitala J. and Kauhanen K. (1989) *EMP, 45,* 187–204. [10] Mège D. and Masson P. (1996) *PSS, 44,* 1499–1546. [11] Heller D.-A. and Janle P. (2000) *EMP, 84,* 1–22. [12] McGovern P. et al. (2001) *JGR, 106,* 23769–23809. [13] Scott E. and Wilson L. (2003) *JGR, 108,* 5035. [14] Zuber M. et al. (1992) *JGR, 97,* 7781–7797. [15] Smith D. et al. (1999) *Science, 284,* 1495–1503. [16] Gwinner K. et al. (2009) *PERS, 75,* 1127–1142. [17] Gwinner K. et al. (2010) *EPSL, 294,* 506–519. [18] Broxton M. and Edwards L. (2008) *LPSC XXXIX,* Abstract #2419. [19] Moratto Z. et al. (2010) *LPSC XXXXI,* Abstract #2364. [20] Schultz R. et al. (2010) *JSG, 32,* 855–875. [21] Polit A. et al. (2009) *JSG, 31,* 662–673. [22] Cailleau B. et al. (2005) *Icarus, 176,* 44–56. [23] Janle P. and Erkul E. (1991) *EMP, 53,* 217–232.